Int. J. Electrochem. Sci., 10 **(2015)** 602 - 624

International Journal of
ELECTROCHEMICAL
SCIENCE
www.electrochemsci.org

Experimental and Theoretical Studies on Corrosion Inhibition Effect of Synthesized Benzothiazole Derivatives on Mild Steel in 15% HCl Solution

Mahendra Yadav[1,*], *Sushil Kumar*[1], *Neelam Kumari*[1], *Indra Bahadur*[2,3], *Eno E. Ebenso*[2,3,*]

[1] Department of Applied Chemistry, Indian School of Mines, Dhanbad, 826004, India
[2] Department of Chemistry, North-West University (Mafikeng Campus), Private Bag X2046, Mmabatho 2735, South Africa
[3] Material Science Innovation & Modelling (MaSIM) Research Focus Area, Faculty of Agriculture, Science and Technology, North-West University (Mafikeng Campus), Private Bag X2046, Mmabatho 2735, South Africa
[*]E-mail: yadav_drmahendra@yahoo.co.in; Eno.Ebenso@nwu.ac.za

Received: 8 October 2014 / *Accepted:* 17 November 2014 / *Published:* 2 December 2014

Two benzothiazole derivatives, namely, (Z)-5-(4-chlorobenzylidene)-3-(benzo[d]thiazol-2-yl)-2-(4-methoxyphenyl)thiazolidine-4-one (CBTMT) and (Z)-5-(4-methoxybenzylidene)-3-(benzo[d]thiazol-2-yl)-2-(4-methoxyphenyl)thiazolidine-4-one (MBTMT) were synthesized in the laboratory and their corrosion inhibition performance on mild steel in 15% HCl solution was studied by means of weight loss measurements, potentiodynamic polarization and electrochemical impedance spectroscopy (EIS) techniques. The inhibition efficiency of each inhibitor increased with increasing the concentration of inhibitor. According to weight loss measurements, the inhibitors CBTMT and MBTMT show corrosion inhibition efficiency of 95.8 and 97.5% respectively, in 150 ppm concentration, at 303 K. Polarization studies showed that corrosion current density decreased in presence of both the inhibitors in comperision to in absence of inhibitors. The thermodynamic adsorption and activation parameters were evaluated for corrosion inhibition process.The adsorption of inhibitors on the mild steel surface obey Langmuir adsorption isotherm. The surface analysis of uninhibited and inhibited mild steel samples was performed by scanning electron microscopy (SEM), energy dispersive X-ray spectroscopy (EDX) and atomic force microscopy (AFM). Quantum chemical parameters calculated by Density functional theory (DFT) were correlated with the experimental results.

Keywords: Mild steel; Benzothiazole derivatives; EIS; Polarization; Corrosion inhibition; DFT

1. INTRODUCTION

The study of corrosion processes and their inhibition by organic inhibitors is a very active field of research [1]. Many researchers reported that the inhibition effect mainly depends on some physico-chemical and electronic properties of the organic inhibitor which relate to its functional groups, steric effects, electronic density of donor atoms, and orbital character of donating electrons, and so on [2, 3]. The inhibiting mechanism is generally explained by the formation of a physically and/or chemically adsorbed film on the metal surface [4, 5]. It is well known that organic compounds which act as good inhibitors are rich in heteroatoms, such as sulphur, nitrogen, and oxygen [6-10]. Both the studied inhibitors MBTMT and CBTMT contain benzothiazole ring. Benzothiazole is a fused heterocyclic molecule and have strong ability of bonding with metal ions via donor atoms (N and S) to form metal complexes. Benzothiazole molecule shows three anchoring sites suitable for surface bonding: the nitrogen atom with its lone pair of electrons, sulfur atom and the aromatic rings [11, 12]. Thus, it is expected that both the studied compounds will show good corrosion inhibition efficiencies.

In continuation of our research for developing corrosion inhibitors [13-15] with low toxicity, high effectiveness and efficiency, the present paper explores a systematic study to ascertain the inhibitive action of synthesized benzothiazole derivatives, namely, (Z)-5-(4-chlorobenzylidene)-3-(benzo[d]thiazol-2-yl)-2-(4-methoxyphenyl)thiazolidine-4-one (CBTMT) and (Z)-5-(4-methoxybenzylidene)-3-(benzo[d]thiazol-2-yl)-2-(4-methoxyphenyl)thiazolidine-4-one (MBTMT) on corrosion of mild steel in 15% HCl solution by using weight loss measurement, potentiodynamic polarization, AC impedance and quantum chemical calculations.

2. EXPERIMENTAL PROCEDURES

2.1. Synthesis of inhibitors

The inhibitors MBTMT and CBTMT were synthesized by the method reported in literature [16]. The synthetic route of inhibitors (CBTMT and MBTMT) is shown in Scheme 1 and structure of inhibitors is shown in Figure 1. The purity of the inhibitors was checked by thin layer chromatography (TLC). The melting point, yield and IR data of the synthesized compounds are given below:

CBTMT
Yield (78%), m.p. = 216-218 °C.
IR (ν/cm^{-1}): 1720 (C=O), 1660 (C=N), 2930 (CH alkyl), 740 (C-S)

MBTMT
Yield (74%), m.p. = 228-230 °C.
IR (ν/cm^{-1}): 1650 (C=N), 1710 (C=O), 2915 (CH alkyl), 740 (C-S)

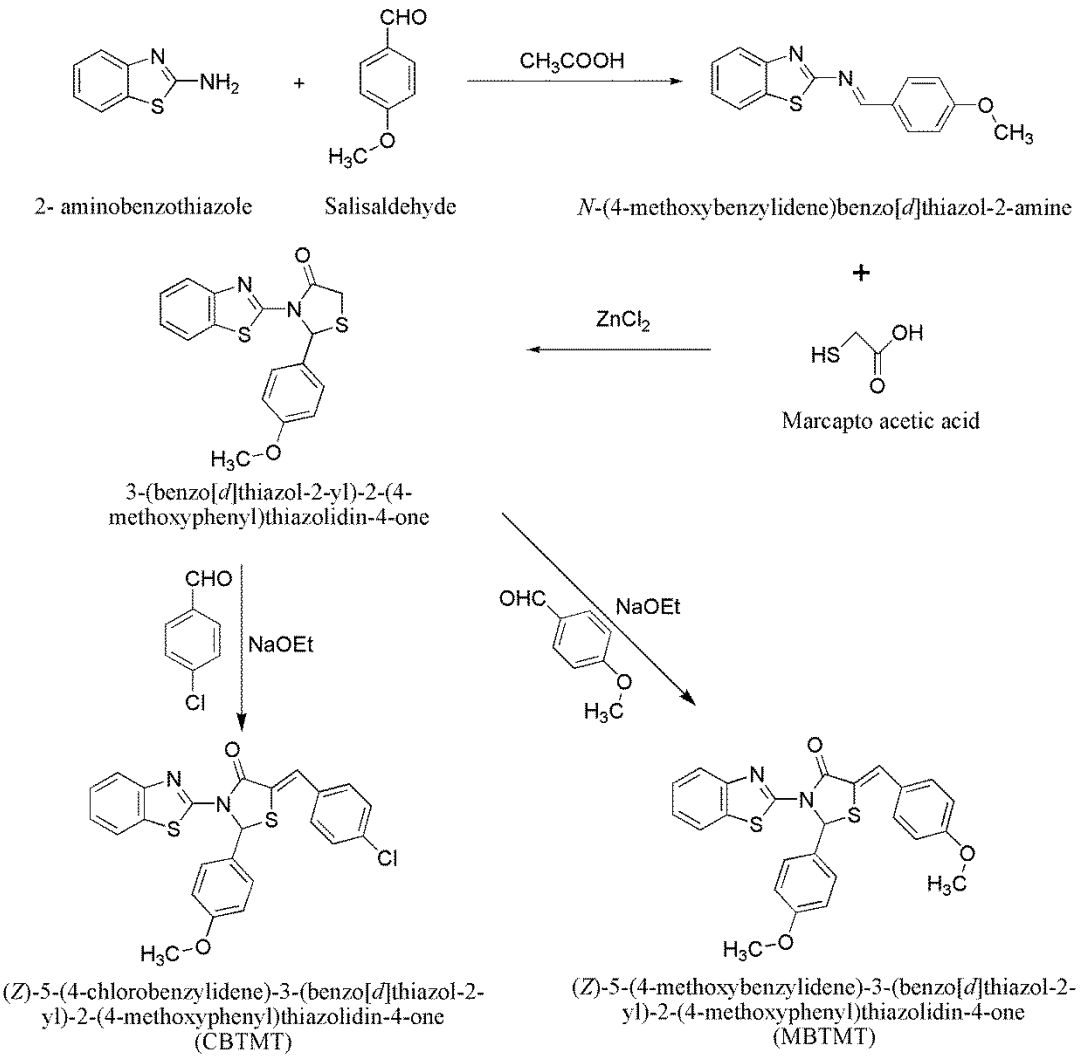

Scheme 1. Synthetic route of inhibitors (Z)-5-(4-chlorobenzylidene)-3-(benzo[d]thiazol-2-yl)-2-(4-methoxyphenyl)thiazolidine-4-one (CBTMT) and (Z)-5-(4-methoxybenzylidene)-3-(benzo[d]thiazol-2-yl)-2-(4-methoxyphenyl)thiazolidine-4-one (MBTMT).

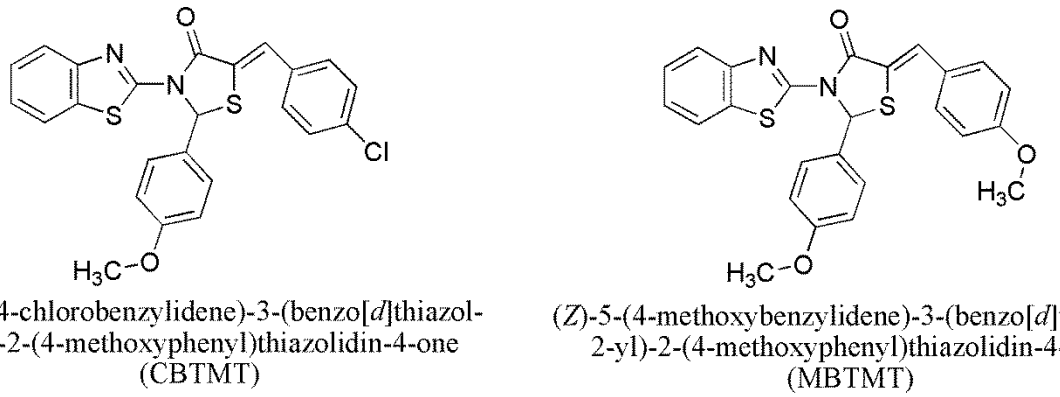

Figure 1. Structure of inhibitors (Z)-5-(4-chlorobenzylidene)-3-(benzo[d]thiazol-2-yl)-2-(4-methoxyphenyl)thiazolidine-4-one (CBTMT) and (Z)-5-(4-methoxybenzylidene)-3-(benzo[d]thiazol-2-yl)-2-(4-methoxyphenyl)thiazolidine-4-one (MBTMT).

2.2. Mild steel sample

The composition (wt.%) of the mild steel sample used for the study was : C, 0.12; Mn, 0.11; Cu, 0.01; Si, 0.02; Sn, 0.01; P, 0.02; Ni, 0.02 and balance Fe. The mild steel samples having dimension 3.0 cm × 3.0 cm × 0.1 cm were mechanically cut and abraded with different grade emery papers (120, 220, 400, 600, 800, 1500 and 2000 grade) for weight loss experiment. For electrochemical measurements mild steel samples having dimension 1.0 cm × 1.0 cm × 0.1 cm were mechanically cut and abraded similarly to the previous procedure, with an exposed area of 1 cm^2 (rest covered with araldite resin) with 3 cm long stem. Prior to the experiment, specimens were washed with distilled water, degreased in acetone, dried and stored in vacuum desiccator.

2.3. Test solution

In the present study, experiments were performed in 15% HCl solution which was prepared in double distilled water using AR grade hydrochloric acid (37% HCl) supplied by Ranbaxy fine chemicals. The concentration range of inhibitors was 25–150 ppm (mg L^{-1}) and the volume of test solution used for weight loss measurement and electrochemical studies was 250 mL and 150 mL, respectively.

2.4. Methods

2.4.1. Weight loss measurements

The apparatus and procedure followed for the weight loss measurements were as previously reported [13-5]. The corrosion rate (*CR*), inhibition efficiency (η%) and surface coverage (θ) were determined by following equations [17]:

$$CR\left(\text{mmy}^{-1}\right) = \frac{8.76\times10^4\times W}{D\times A\times t} \quad (1)$$

where, W = weight loss (g), A = area of specimen (cm^2) exposed in solution, t = exposure time (h), and D = density of mild steel (g cm^{-3}).

$$\theta = \frac{CR_0 - CR_i}{CR_0} \quad (2)$$

$$\eta(\%) = \frac{CR_0 - CR_i}{CR_0}\times100 \quad (3)$$

where, CR_0 and CR_i are corrosion rate in absence and presence of inhibitors.

2.4.2. Electrochemical Measurements

Potentiodynamic polarization measurements were carried out in a conventional three-electrode cell consisting of mild steel working electrode (WE), a platinum counter electrode (CE) and a saturated calomel electrode (SCE) as reference electrode, using CH electrochemical workstation (Model No:

CHI 760D, manufactured by CH Instruments, Austin, USA) at 30 ºC. After establishment of the open circuit potential, potentiodynamic polarization curves were obtained with a scan rate of 1 mVs^{-1} in the potential range from -300 to +300 mV. Corrosion current density (i_{corr}) values were obtained by Tafel extrapolation method. All potentials were measured against SCE. The percentage inhibition efficiency (η %), was calculated using the equation

$$\eta(\%) = \frac{i^0_{corr} - i_{corr}}{i^0_{corr}} \times 100 \quad (1)$$

where, i^0_{corr} and i_{corr} are the values of corrosion current density in absence and presence of inhibitors, respectively.

Electrochemical impedance measurements were carried out using the same electrochemical cell and electrochemical workstation as mentioned above in the frequency range from 0.1 to 10000 Hz using amplitude of 10 mV peak to peak with an ac signal at the open-circuit potential. The impedance data such as solution resistance (R_s), charge transfer resistance (R_{ct}) and CPE constants (Y_0 and n) were obtained by fitting the experimental data in appropriate equivalent circuit. The inhibition efficiency (η %) was calculated by using the following relation:

$$\eta(\%) = \frac{R_{ct(inh)} - R_{ct}}{R_{ct(inh)}} \times 100 \quad (5)$$

where $R_{ct(inh)}$ and R_{ct} are charge transfer resistance in the absence and presence of inhibitor respectively. The values of electrochemical double layer capacitance (C_{dl}) were calculated by using the following equation [18]:

$$C_{dl} = (Y_0 R_{ct}^{1-n})^{1/n} \quad (6)$$

where Y_0 is CPE constant and n is CPE exponent . The value of n represents the deviation from the ideal behavior and it lies between 0 and 1.

2.4.3. Scanning electron microscopic and energy dispersive spectroscopy analysis

For surface morphological study of the uninhibited and inhibited mild steel samples, SEM and EDX images were recorded using the instrument HITACHI S3400N.

2.4.4. Atomic Force Microscopy

The AFM images of polished, uninhibited and inhibited mild steel samples were carried out using a Nanosurf Easyscan2 instrument, Model: NT-MDT, Russia; Solver Pro-47.

2.4.5. Quantum chemical study

Complete geometrical optimizations of the investigated molecules were performed using density functional theory (DFT) in aqueous phase with the Becke's three parameter exchange functional along with the Lee–Yang–Parr nonlocal correlation functional (B3LYP) with 6-31G (d, p) basis set as implemented in Gaussian 03 program package [19]. Theoretical parameters such as the

energies of the highest occupied and lowest unoccupied molecular orbital (E_{HOMO} and E_{LUMO}), energy gap (ΔE) and dipole moment (μ) were determined.

3. RESULTS AND DISCUSSION

3.1. Weight loss measurements

3.1.1. Effect of inhibitor concentration and temperature

Corrosion parameters calculated by weight loss measurements after 6 h of immersion time at different temperatures ranging from 303K to 333K are given in Table 1. From Table 1, it is apparent that inhibition efficiency increased with increasing the concentration of the inhibitors and decreased on increasing the temperature. The increase in inhibition efficiency with increasing concentration of inhibitors is due to increase in the surface coverage, resulting retardation of metal dissolution [20]. The decrease in inhibition efficiency with increasing temperature can be described on the basis that the increase in temperature leads to a shift of the equilibrium constant towards desorption of the inhibitors molecules at the surface of mild steel [21, 22).

Table 1. Corrosion parameters of mild steel in 15% HCl solution in the presence and absence of inhibitor at different temperature, obtained from weight loss measurements.

	303 K			313 K			323 K			333 K		
Conc. (ppm)	*CR* (mmy^{-1})	θ	η %	*CR* (mmy^{-1})	θ	η %	*CR* (mmy^{-1})	θ	η %	*CR* (mmy^{-1})	θ	η %
Blank	28.2	-	-	58.1	-	-	98.9	-	-	144.5	-	-
CBTMT												
25	4.65	0.83	83.5	10.69	0.81	81.6	19.38	0.80	80.4	29.76	0.79	79.4
50	3.72	0.86	86.8	8.88	0.84	84.7	16.22	0.83	83.6	25.14	0.82	82.6
75	2.70	0.90	90.4	6.79	0.88	88.3	12.65	0.87	87.2	19.94	0.86	86.2
100	1.80	0.93	93.6	4.93	0.91	91.5	9.59	0.90	90.3	15.46	0.89	89.3
150	1.18	0.95	95.8	3.72	0.93	93.6	7.41	0.92	92.5	12.28	0.91	91.5
MBTMT												
25	3.86	0.86	86.0	9.29	0.84	84.0	16.81	0.83	83.0	25.86	0.82	82.1
50	2.48	0.91	91.2	6.33	0.89	89.1	11.67	0.88	88.2	18.92	0.86	86.9
75	2.11	0.92	92.5	5.57	0.90	90.4	10.58	0.89	89.3	17.19	0.88	88.1
100	1.24	0.95	95.6	3.83	0.93	93.4	7.41	0.92	92.5	12.57	0.91	91.3
150	0.70	0.97	97.5	2.78	0.95	95.2	5.73	0.94	94.2	9.82	0.93	93.2

Both the inhibitors are good inhibitors even at the concentration as low as 25 ppm. The inhibition efficiency of MBTMT was found to be higher than CBTMT. The maximum inhibition efficiency offered by MBTMT was 86.0% and 97.5% at 25 ppm and 150 ppm respectively at 303 K (Table1).

3.1.2. Thermodynamic and activation parameters

The temperature dependence of the corrosion rate can be expressed by Arrhenius equation. This equation can be represented graphically by plotting natural logarithm of the corrosion rates vs. 1/T without and with addition of various concentrations of inhibitor. The apparent activation energy (E_a) for dissolution of mild steel in 15% HCl solution was calculated by using Arrhenius equation:

$$\log CR = \frac{-E_a}{2.303RT} + \log A \qquad (4)$$

where R is the molar gas constant (8.314 J $K^{-1}mol^{-1}$), T is the absolute temperature (K) and A is the Arrhenius pre-exponential factor. Figure 2 presents the Arrhenius plot of log CR against $1/T$ for the corrosion of mild steel in 15% HCl solution in the absence and presence of inhibitors at concentrations ranging from 25 to 150 ppm. From the slope of Figure 2, the values of E_a were calculated and summarized in Table 2. It is evident from Table 2 that the values of the apparent activation energy for the inhibited solutions were higher than that for the uninhibited solution. The higher values of apparent activation energy (E_a) in the presence of inhibitor as compared to the E_a in the absence of inhibitor in 15% HCl solution indicates that the inhibitor induces the energy barrier for the corrosion reaction which leads to the decreasing of rate of corrosion of mild steel in the present of inhibitor. It is also seen that the values of E_a increased with an increase in inhibitor concentrations, a phenomenon which indicates that the adsorption of the inhibitor onto mild steel surface was favourable with increasing inhibitor concentrations [23].

The values of standard enthalpy of activation (ΔH^*) and standard entropy of activation (ΔS^*) were calculated by using the transition state equation

$$CR = \frac{RT}{Nh}\exp\left(\frac{\Delta S^*}{R}\right)\exp\left(-\frac{\Delta H^*}{RT}\right) \qquad (5)$$

where, h is Planck's constant and N is the Avogadro number, respectively.

A plot of log (CR/T) against $1/T$ (Figure 3) gave straight lines with a slope of $-\Delta H^*/2.303R$ and an intercept of [log(R/Nh) + ($\Delta S^*/2.303R$)], from which the activation thermodynamic parameters (ΔH^* and ΔS^*) were calculated, as listed in Table 2.

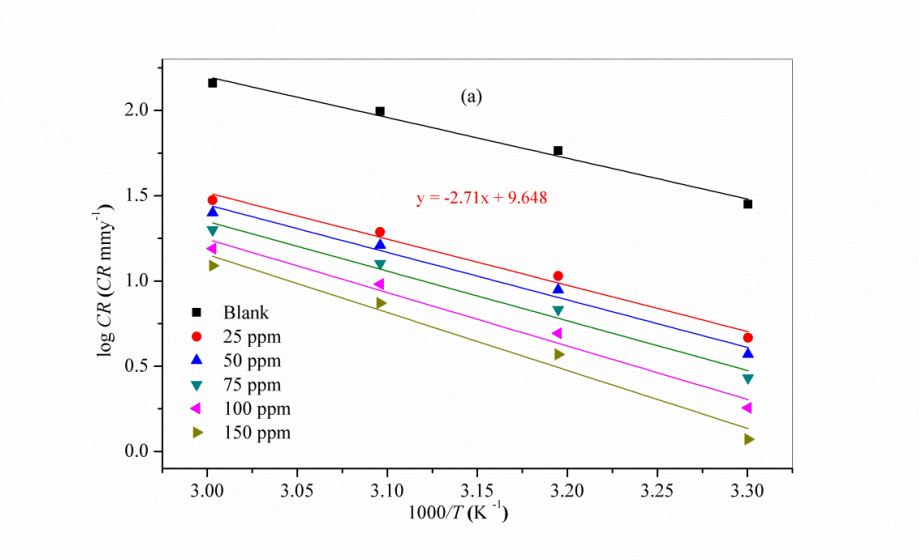

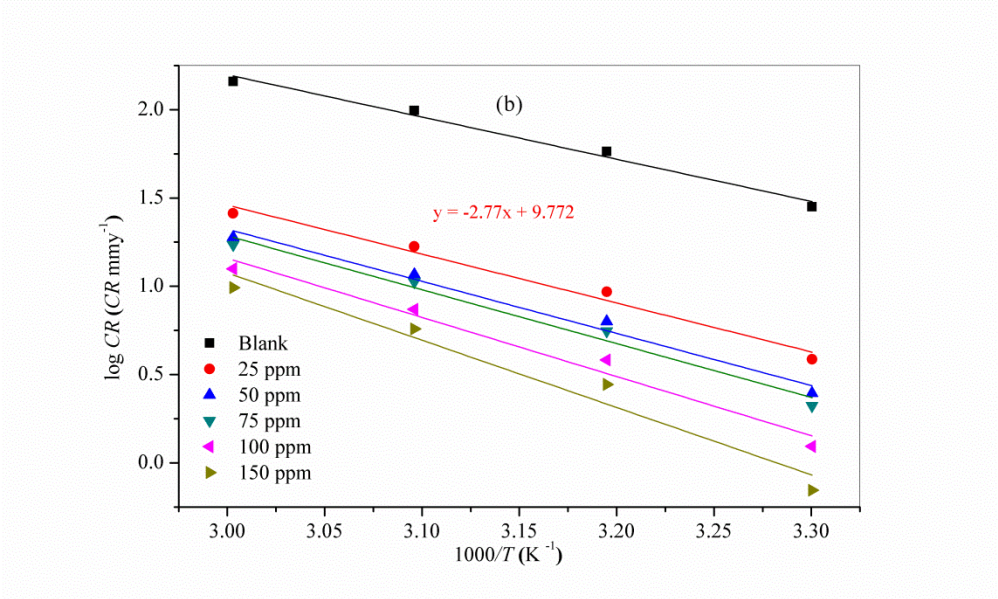

Figure 2. Arrhenius plots of log *CR* versus 1000/*T* for mild steel corrosion in 15% HCl solution (a) CBTMT (b) MBTMT.

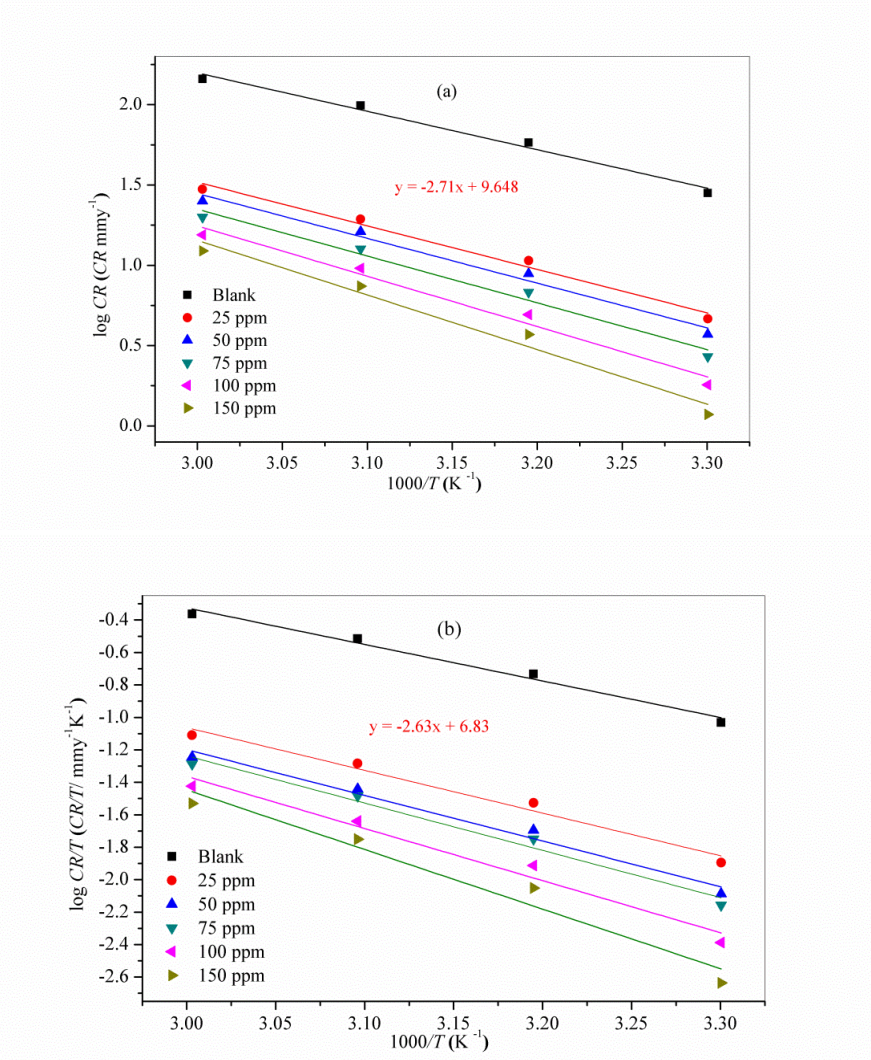

Figure 3. Transition state plot of log *CR* /*T* versus 1000/*T* for mild steel in 15% HCl solution at different concentration (a) CBTMT (b) MBTMT.

The negative value of ΔS^* for both inhibitors indicates that the formation of the activated complex in the rate determining step represents an association rather than a dissociation step, meaning that a decrease in disorder takes place during the course of the transition from reactants to activated complex [24].

Table 2. Activation parameter for mild steel in 15% HCl solution in the absence and presence of inhibitor obtained from weight loss measurements

Inhibitor	Concentration (ppm)	E_a ($kJmol^{-1}$)	ΔH^* ($kJ\ mol^{-1}$)	ΔS^* ($Jmol^{-1}K^{-1}$)
Blank	-	45.7	43.0	-74.5
CBTMT	25	51.8	49.2	-69.1
	50	53.2	50.7	-66.0
	75	55.7	53.0	-60.6
	100	59.9	57.2	-50.1
	150	65.1	62.4	-36.7
MBTMT	25	53.0	50.3	-66.8
	50	56.5	53.8	-58.9
	75	58.4	55.7	-53.9
	100	64.1	61.5	-39.4
	150	72.9	70.3	-24.1

3.1.3. Adsorption isotherm

The effectiveness of these inhibitors may be explained assuming the adsorption as the cause of the inhibition. The extent of adsorption of different inhibitors at a fixed concentration would depend upon the surface area of the inhibitor molecules, the number of active centers such as N, S and O atoms and the intensities of lone pairs of electrons on these sites along with the intensities of π-electrons on aromatic rings. The plots of C_{inh}/θ vs. C_{inh} yielded straight lines [Fig. 4] with correlation coefficient (R^2) and slope values given in Table 3 at different temperatures. The correlation coefficient and slope values in Table 3 are near to unity indicating that the adsorption of both the inhibitors obey Langmuir adsorption isotherm represented by the following equation:

$$\frac{C_{\text{inh}}}{\theta} = \frac{1}{K_{\text{ads}}} + C_{\text{inh}} \quad (6)$$

where C_{inh} is the inhibitor concentration, K_{ads} is the equilibrium constant for adsorption-desorption process.

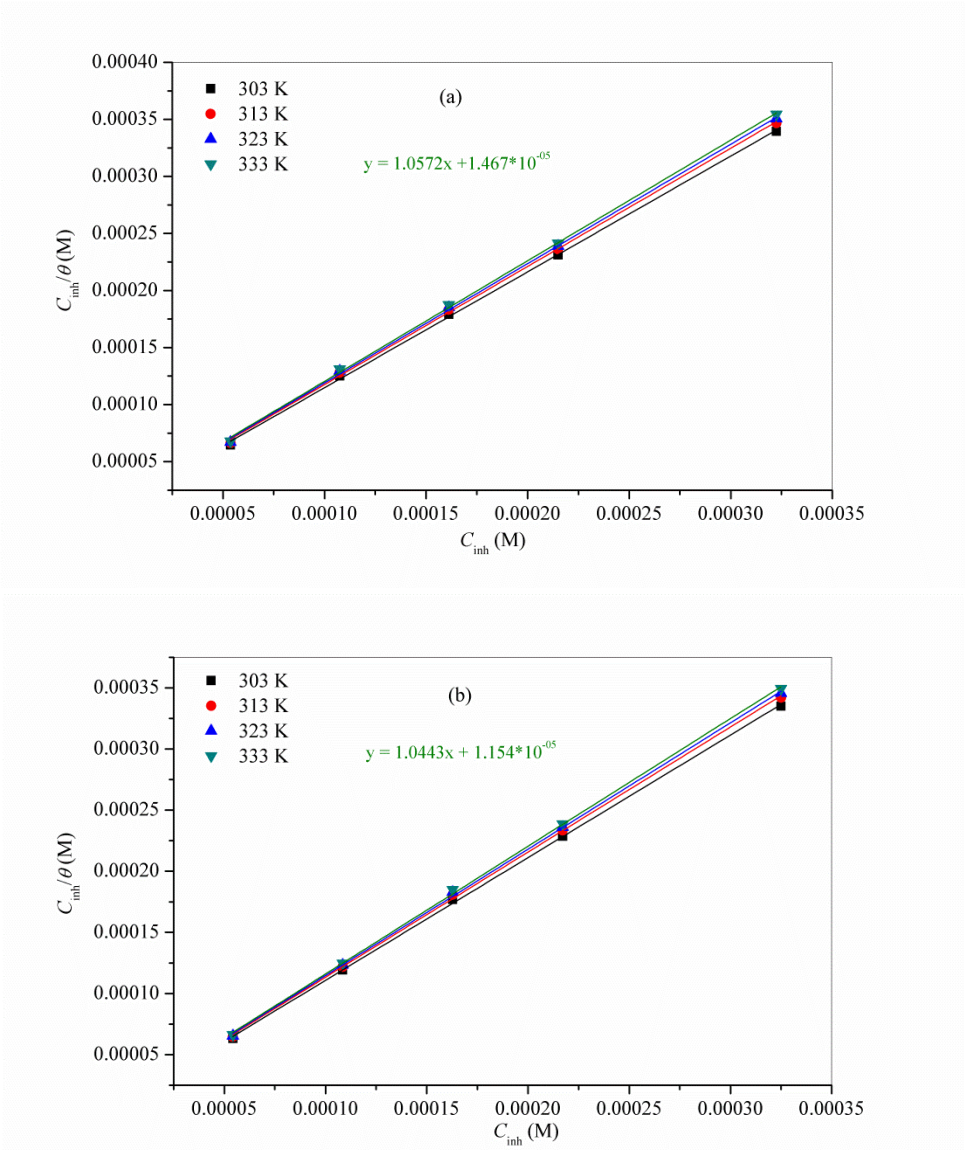

Figure 4. Langmuir plots of (C_{inh}/θ) versus C_{inh} for (a) CBTMT (b) MBTMT.

The values of K_{ads} were calculated from the intercept of Figure 4. Large values of K_{ads} obtained for both studied inhibitors suggesting more efficient adsorption and hence better corrosion inhibition efficiency. Using the values of K_{ads} , the values of $\Delta G^{\circ}_{\text{ads}}$ were obtained by using the following equation:

$$\Delta G^{0}_{\text{ads}} = -RT \ln\left(55.5 K_{\text{ads}}\right) \quad (7)$$

The value of 55.5 is the concentration of water in solution in mol L^{-1}.

Table 3. Adsorption parameters for CBTMT and MBTMT calculated from Langmuir adsorption isotherm for mild steel in 15% HCl solution at a temperature range of 303-333K

Inhibitor	Temperature (K)	K_{ads} (M^{-1})	ΔG°_{ads} (kJ mol^{-1})	Correlation coefficient (R^2)	Slope values
CBTMT	303	7.46×10^4	-38.4	0.999	1.01
	313	7.13×10^4	-39.5	0.999	1.03
	323	6.97×10^4	-40.7	0.999	1.04
	333	6.81×10^4	-41.9	0.999	1.05
MBTMT	303	9.45×10^4	-38.9	0.999	1.00
	313	9.05×10^4	-40.1	0.999	1.02
	323	8.85×10^4	-41.3	0.999	1.03
	333	8.65×10^4	-42.5	0.999	1.04

The calculated values of K_{ads} and ΔG°_{ads} are listed in Table 3. The negative values of ΔG°_{ads} indicate spontaneous adsorption of inhibitor molecules on the mild steel surface and strong interactions between inhibitor molecules and the metal surface . In general, values of ΔG°_{ads} up to −20 $kJmol^{-1}$ are compatible with physisorption and those which are more negative than −40 $kJmol^{-1}$ involve chemisorptions [25]. The calculated ΔG°_{ads} values for AMPO and MMPA were found in the range of -38.4 to –41.9 and -38.9 to –42.5 $kJmol^{-1}$, respectively, at different temperatures (303-333 K), these values were between the threshold values for physical adsorption and chemical adsorption, indicating that the adsorption process of inhibitors at mild steel surface involve both the physical as well as chemical adsorption.

3.2. Electrochemical studies

3.2.1. Polarization studies

The effect of addition of inhibitors on the anodic and cathodic polarization curves for mild steel in 15% HCl solution was studied and polarization curves are shown in Figure 5 (a, b) at 303 K. The values of cathodic (β_c) and anodic (β_a) Tafel slopes were calculated from the linear region of the polarization curves. The corrosion current density (i_{corr}) was determined from the intersection of the linear parts of the anodic and cathodic curves with the open circuit corrosion potential (E_{corr}). The corrosion parameters such as corrosion potential (E_{corr}), anodic Tafel slope (β_a), cathodic Tafel slope (β_c), corrosion current density (i_{corr}) and percentage inhibition efficiency (η %) obtained from these curves are given in Table 4.

The results revealed that increasing concentration of both inhibitors resulted in a decrease in corrosion current densities and an increase in inhibition efficiency (η %), suggesting the adsorption of inhibitor molecules at the surface of mild steel to form protective film on mild steel surface [26]. The efficiencies of the inhibitors are in the order: MBTMT > CBTMT at 303 K. The presence of inhibitor cause change in E_{corr} values with respect to the E_{corr} value in absence of inhibitor.

Table 4. Electrochemical parameter and percentage inhibition efficiency (η *%)* obtained from polarisation studies for mild steel in 15% HCl solution in the absence and presence of inhibitor at 303 K.

Inhibitor	Conc (ppm)	$-E_{corr}$ (mV/SCE)	i_{corr} (μA cm^{-2})	β_a (mVdec^{-1})	$-\beta_c$ (mV dec^{-1})	η(%)
Blank	-	416	6733	332	338	-
CBTMT	25	512	1054	357	289	84.3
	50	511	808	264	286	88.0
	75	508	592	274	272	91.2
	100	517	390	300	278	94.2
	150	515	209	328	267	96.9
MBTMT	25	511	841	286	290	87.5
	50	510	565	286	264	91.6
	75	510	451	296	277	93.3
	100	526	255	298	267	96.2
	150	527	128	338	287	98.1

If the displacement in E_{corr} in presence of inhibitor is more than ±85 mV/SCE relating to E_{corr} of the blank, the inhibitor can be considered as a cathodic or anodic type [27, 28]. If the change in E_{corr} is less than ±85 mV the corrosion inhibitor may be regarded as a mixed type. This implies that the inhibitors act as mixed type inhibitor, affecting both anodic and cathodic reactions. The maximum displacement in our study is 111 mV, which indicates that MBTMT and CBTMT act as cathodic inhibitor.

3.2.2. EIS studies

The Nyquist plots for mild steel obtained at mild steel / 15% HCl solution interface with and without the different concentrations of CBTMT and MBTMT at 303 K are shown in Figure 6 (a, b). The existence of a depressed semicircle with its center below the axis ($Z^{'}$) in Nyquist plots (Fig.6 a, b) for both inhibitors suggesting the non-homogeneity and roughness of the mild steel surface [29]. The EIS spectra of all tests were analyzed using the equivalent circuit shown in Figure 7, which is a parallel combination of the charge transfer resistance (R_{ct}) and the constant phase element (CPE), both in series with the solution resistance (R_s). This type of electrochemical equivalent circuit was reported previously to model the iron/acid interface [30]. Constant phase element (CPE) is introduced instead of pure double layer capacitance to give more accurate fit as the double layer at interface does not behave as ideal capacitor.

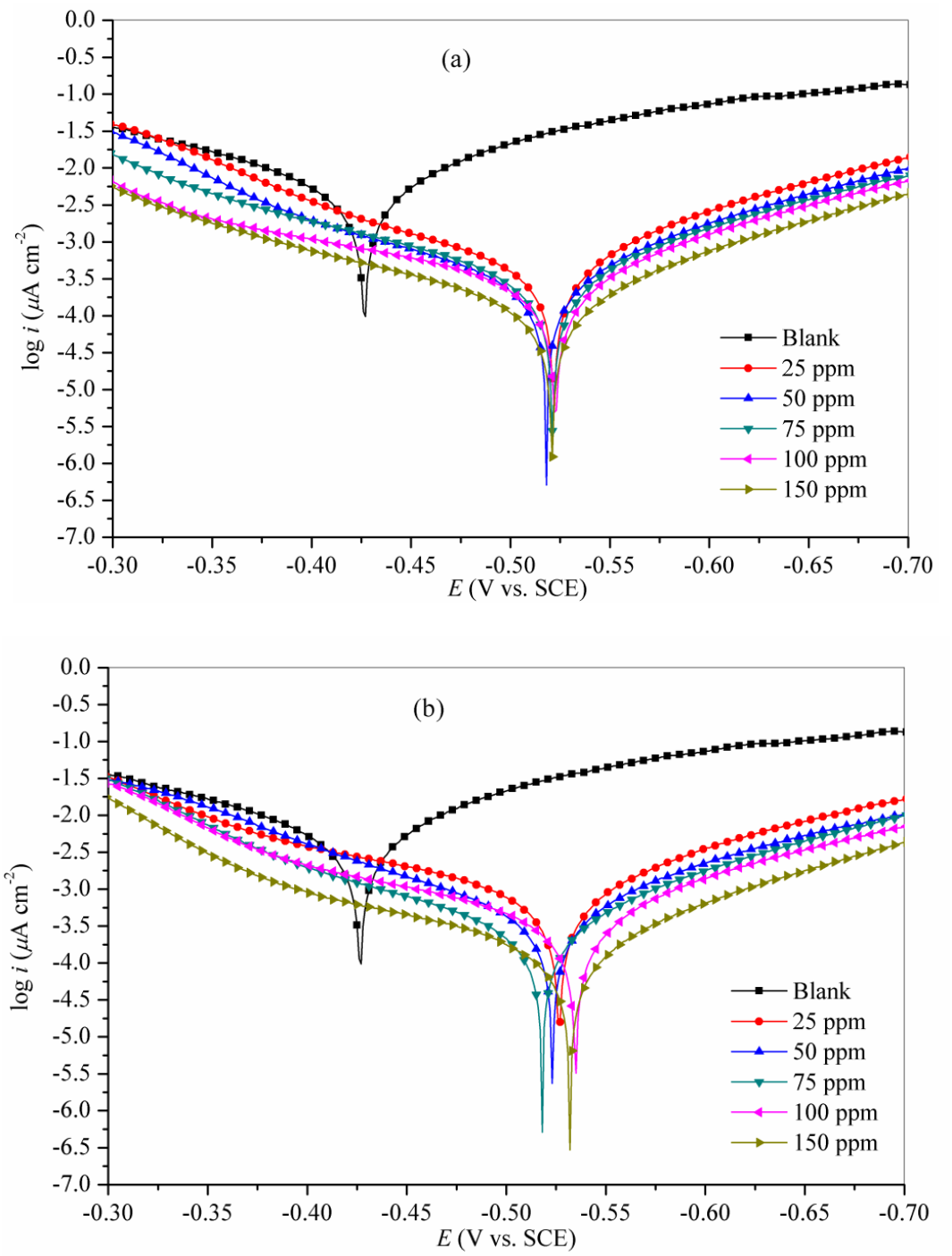

Figure 5. Potentiodynamic polarization curves for mild steel in 15% HCl solution in the presence and absence of inhibitor 303 K (a) CBTMT (b) MBTMT.

The electrochemical parameters such as solution resistance, charge transfer resistance and CPE constants (Y_0 and n) obtained from the fitting the experimental data of Nyquist plots in the equivalent circuit shown in Fig. 7 are presented in Table 5.

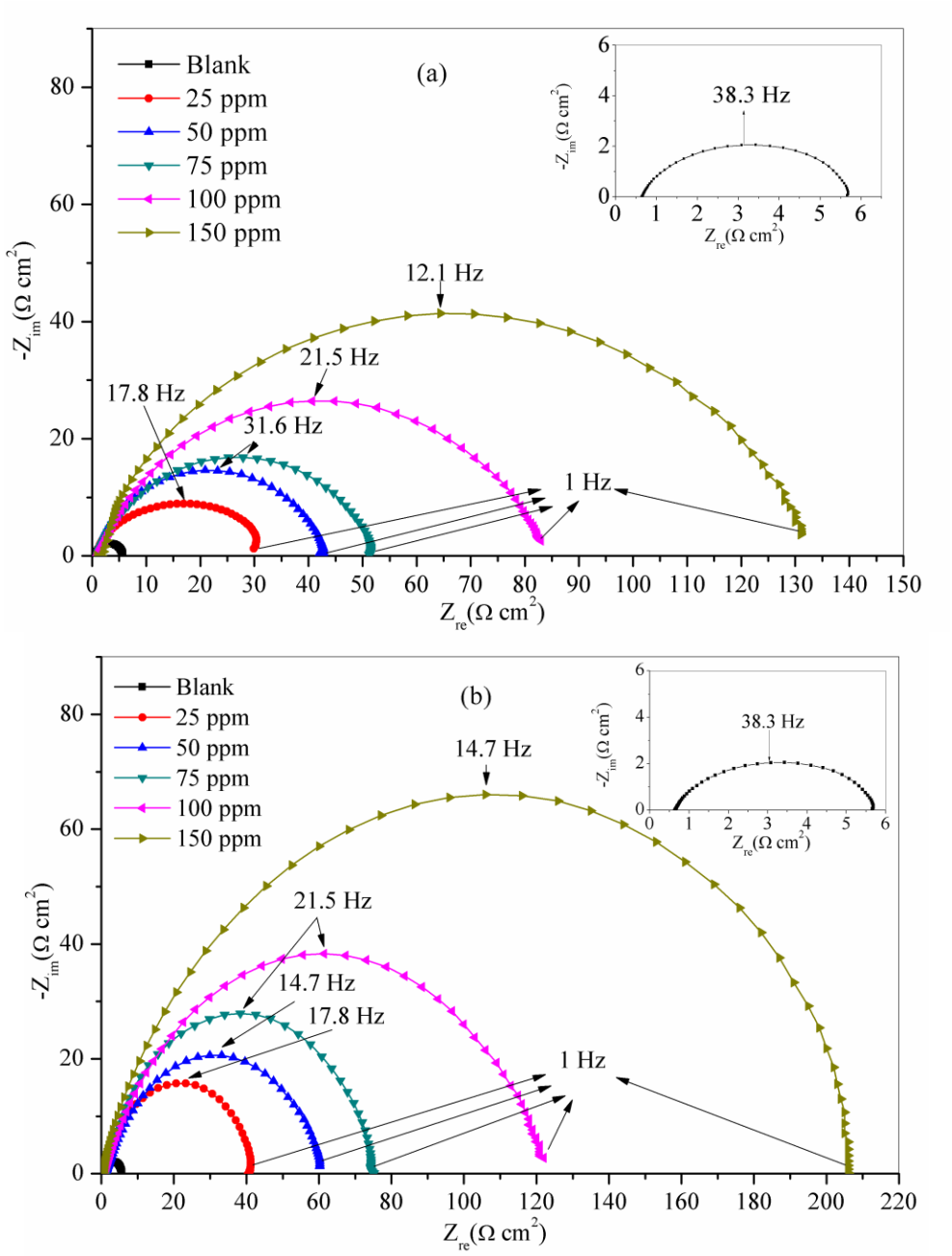

Figure 6. Nyquist plots for mild steel in 15% HCl solution (a) CBTMT (b) MBTMT containing various concentrations at 303K.

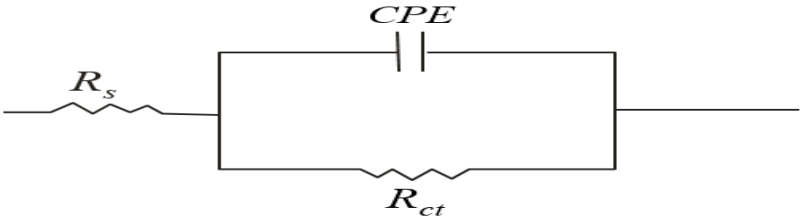

Figure 7. Equivalent circuit diagram

Table 5. Electrochemical impedance parameters for mild steel in 15% HCl solution in the absence and presence of inhibitor at different concentration at 303K.

Inhibitor	Conc.(ppm)	R_s (Ω cm^2)	R_{ct} (Ω cm^2)	Y_o(μF cm^{-2})	n	C_{dl} (μF cm^{-2})	η%
Blank	-	0.65	5.1	1471	0.87	721.1	-
CBTMT	25	0.86	31.0	684	0.78	240.4	83.5
	50	0.86	42.0	309	0.82	124.9	87.8
	75	0.98	51.0	245	0.83	101.5	90.0
	100	1.02	82.0	183	0.84	82.5	93.8
	150	0.97	130.0	100	0.87	52.6	96.0
MBTMT	25	0.90	42.0	495	0.79	185.6	87.8
	50	1.03	61.5	318	0.80	119.4	91.7
	75	0.86	74.0	232	0.81	90.8	93.1
	100	0.96	123.0	148	0.82	64.3	95.8
	150	0.27	208.0	73	0.83	31.2	97.6

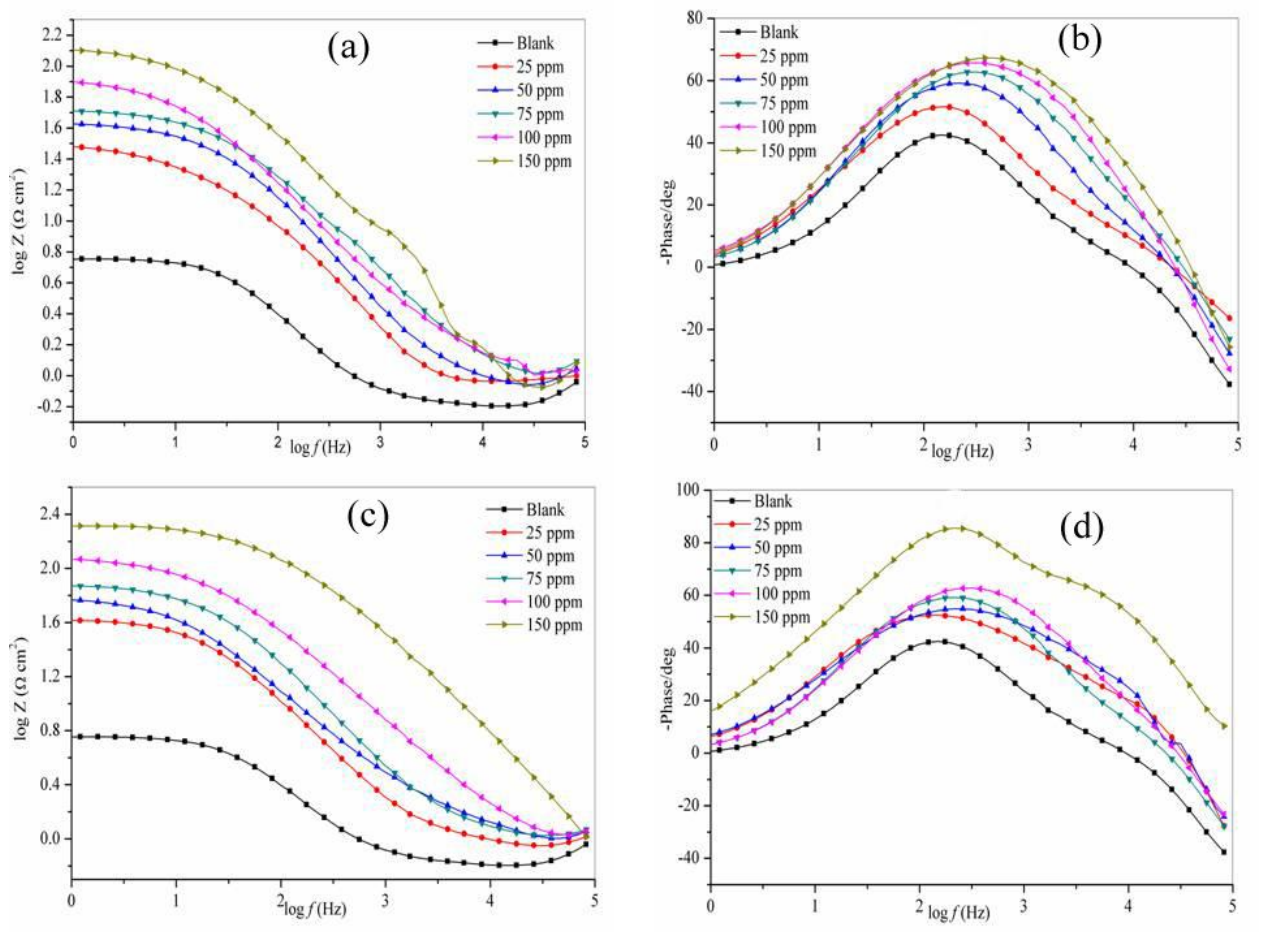

Figure 8. Bode plots for mild steel in a 15% HCl solution in the absence and presence of different concentrations of inhibitors (a, b) CBTMT (c, d) MBTMT.

The data shown in Table 5 reveal that the value of R_{ct} increases with addition of inhibitors as compared to the blank solution, the increase in R_{ct} value is attributed to the formation of a protective film at the metal/solution interface. The C_{dl} value decreases on increasing the concentration of both the inhibitors, indicating the decrease in local dielectric constant and/or to an increase in the thickness of the electrical double layer, suggesting that the inhibitor molecules are adsorbed at the metal/solution interface [31].

The Bode phase angle plots (Figs. 8 b, d) show single maximum (one time constant) at intermediate frequencies, broadening of this maximum in presence of inhibitors accounts for the formation of a protective layer on the electrode surface. The higher values of phase angle for inhibited solution than uninhibited solution reflect the inhibitive action of inhibitors.Figures 8 (a, c) show that the impedance value in the presence of both inhibitors is larger than in absence of inhibitors and the value of impedance increases on increasing the concentration of both studied inhibitors. These indicate that the corrosion rate is reduced in presence of the inhibitors and continued to decreasing on increasing the concentration of inhibitors.

Electrochemical results (η %) are in good agreement with the results (η %) obtained by weight loss experiment.

3.3. Scanning electron microscopy

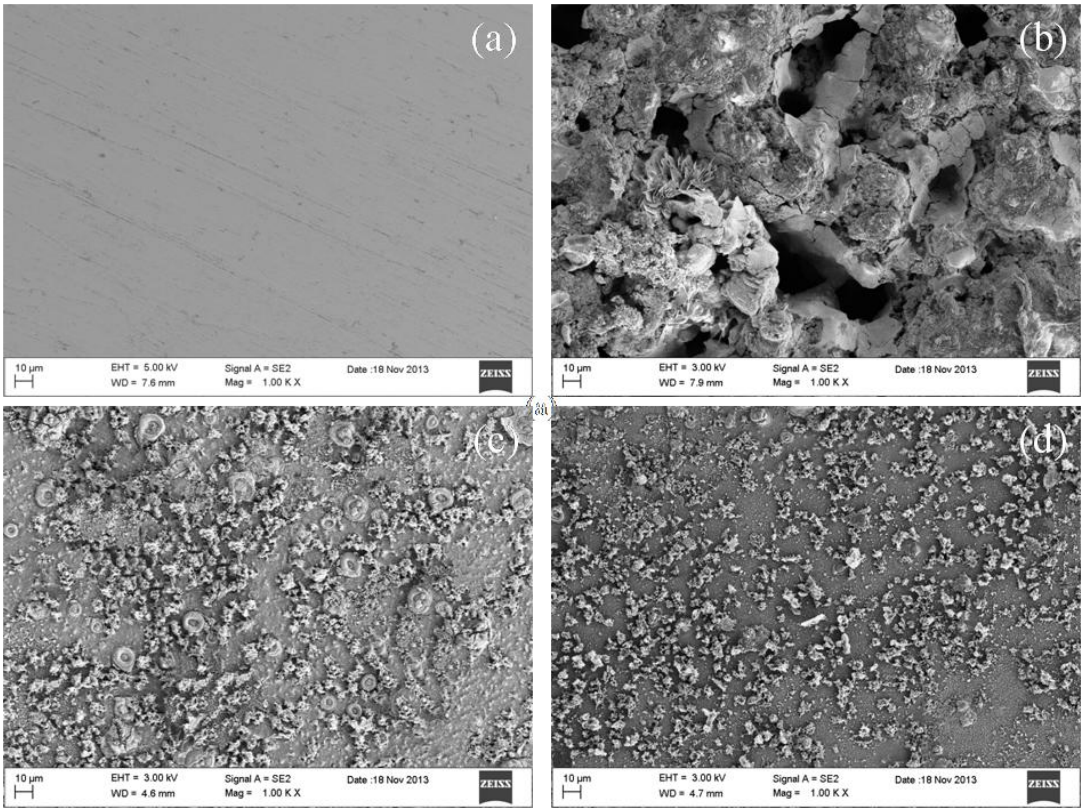

Figure 9. SEM image of mild steel in 15% HCl solution after 6h immersion at 303K (a) before immersion (polished) (b) After immersion without inhibitor (c) with inhibitor CBTMT (d) with inhibitor MBTMT.

SEM photomicrographs for mild steel in 15% HCl solution in the absence and presence of 150 ppm of CBTMT and MBTMT are shown in Figure 9 (a-d).

The surface of the polished mild steel specimen (Fig. 9 a) is very smooth and shows no corrosion while mild steel specimen dipped in 15% HCl solution in the absence of inhibitor (Fig. 9 b) is very rough and the surface is damaged due to metal dissolution. However, the presence of 150 ppm of inhibitor suppresses the rate of corrosion and surface damage has been diminished considerably (Figs. 9 c, d) as compared to the blank solution (Fig. 9 b), suggesting formation of a protective inhibitor film at the mild steel surface.

3.4. Energy dispersive spectroscopy

Energy dispersive X-ray analysis (EDX) technique was employed in order to get information about the composition of the surface of the mild steel sample in absence and presence of inhibitors in 15% HCl solution. The EDX spectra of uninhibited and inhibited mild steel samples are shown in Figure 10 (a, b, c, d).

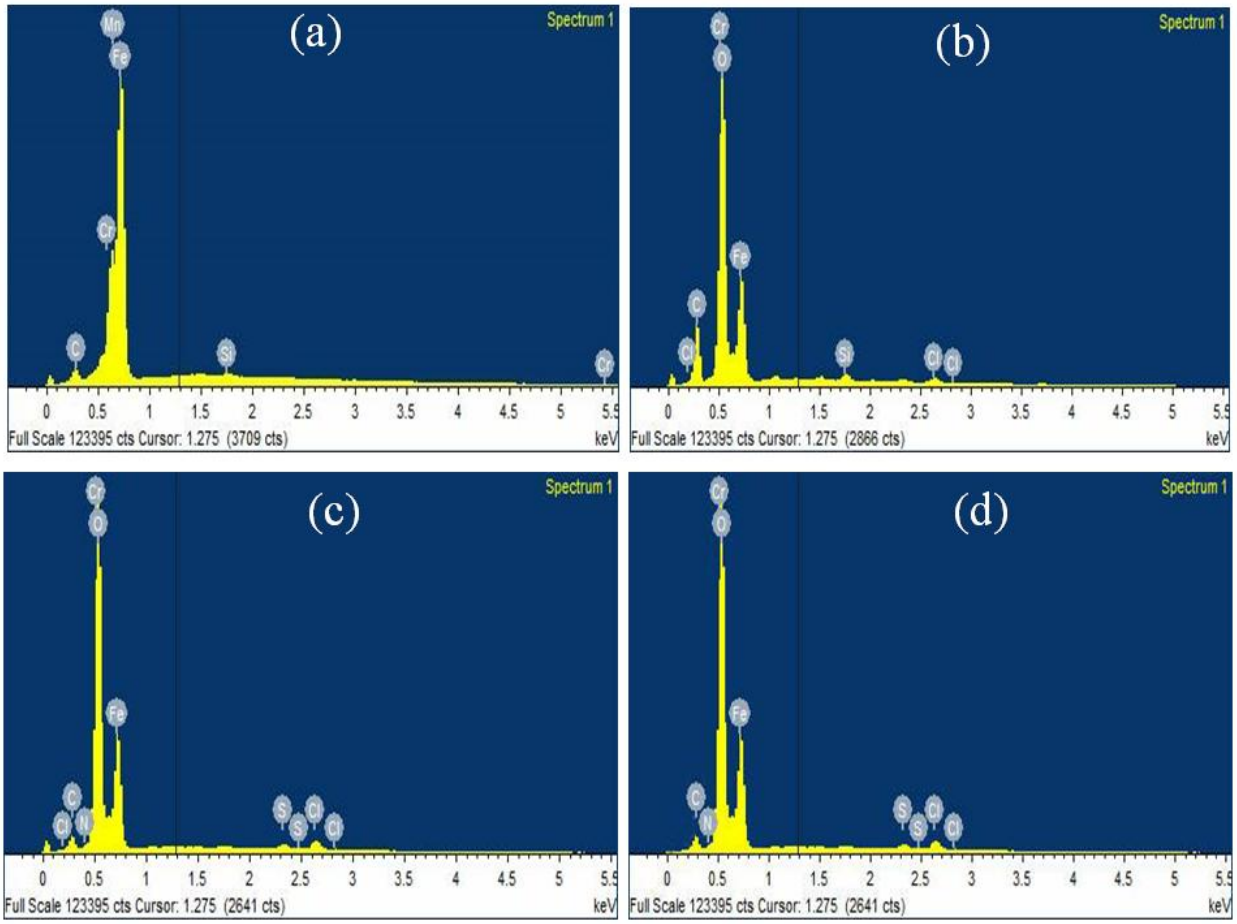

Figure 10. EDX spectra of mild steel specimens (a) polished (b) After immersion without inhibitor (c) with 150 ppm CBTMT (d) with 150 ppm MBTMT.

The percentage atomic content of various elements of the polished, uninhibited and inhibited mild steel surface determined by EDX is shown in Table 6. The percentage atomic content of Fe for mild steel immersed in 15% HCl solution is 83.12%, and those for mild steel dipped in an optimum concentration (150 ppm) of CBTMT, and MBTMT are 67.14% and 61.18%, respectively. From Figure 10, the spectra of inhibited samples show that the Fe peaks are considerably suppressed, when compared with the polished and uninhibited mild steel sample. This suppression of Fe lines is due to the inhibitory film formed on the mild steel surface. The EDX spectra of inhibited mild steel contains the peaks corresponding to all the elements present in the inhibitor molecules indicating the adsorption of inhibitor molecules at the surface of mild steel.

Table 6. Percentage atomic contents of elements obtained from EDX spectra.

Inhibitors	Fe	C	Cr	Mn	Cl	N	O
Polished mild Steel	85.26	12.46	0.86	0.46	-	-	-
Mild steel in blank HCl	83.12	15.68	0.67	0.28	2.29	-	6.36
Mild steel in CBTMT	67.14	17.36	0.58	-	0.35	3.65	8.46
Mild steel in MBTMT	61.18	17.72	0.57	-	0.33	4.16	11.64

3.5. Atomic force microscopy

The three-dimensional AFM images of polished, uninhibited and inhibited mild steel samples are shown in Figure 11 a-d. The average roughness of polished mild steel sample (Fig. 11 a) and mild steel sample in 15% HCl solution without inhibitor (Fig. 11 b) were found as 25 and 650 nm. It is clearly shown in Figure 11(b) that mild steel sample is badly damaged due to the acid attack on surface. However, in presence of optimum concentration (150 ppm) of CBTMT and MBTMT as shown in Figure 11 (c, d), the average roughness were reduced to 82 and 68 nm, respectively. The lower value of roughness for MBTMT than CBTMT reveals that MBTMT protects the mild steel surface more efficiently than CBTMT in 15% HCl solution.

3.6. Theoretical calculation

In order to study the effect of molecular structure on the inhibition efficiency, quantum chemical calculations were performed by using DFT and all the calculations were carried out with the help of complete geometry optimization. Optimized structure, E_{HOMO} and E_{LUMO} are shown in Figure12 (a, b). The quantum chemical parameters such as the energy of the highest occupied molecular orbital (E_{HOMO}), the energy of the lowest unoccupied molecular orbital (E_{LUMO}), energy gap (ΔE), dipole moment (μ), absolute electronegativity (χ), global hardness (γ) and softness (σ) and fraction of electrons transferred from the inhibitor molecule to the metal surface (ΔN) were determined and summarized in Table 7.

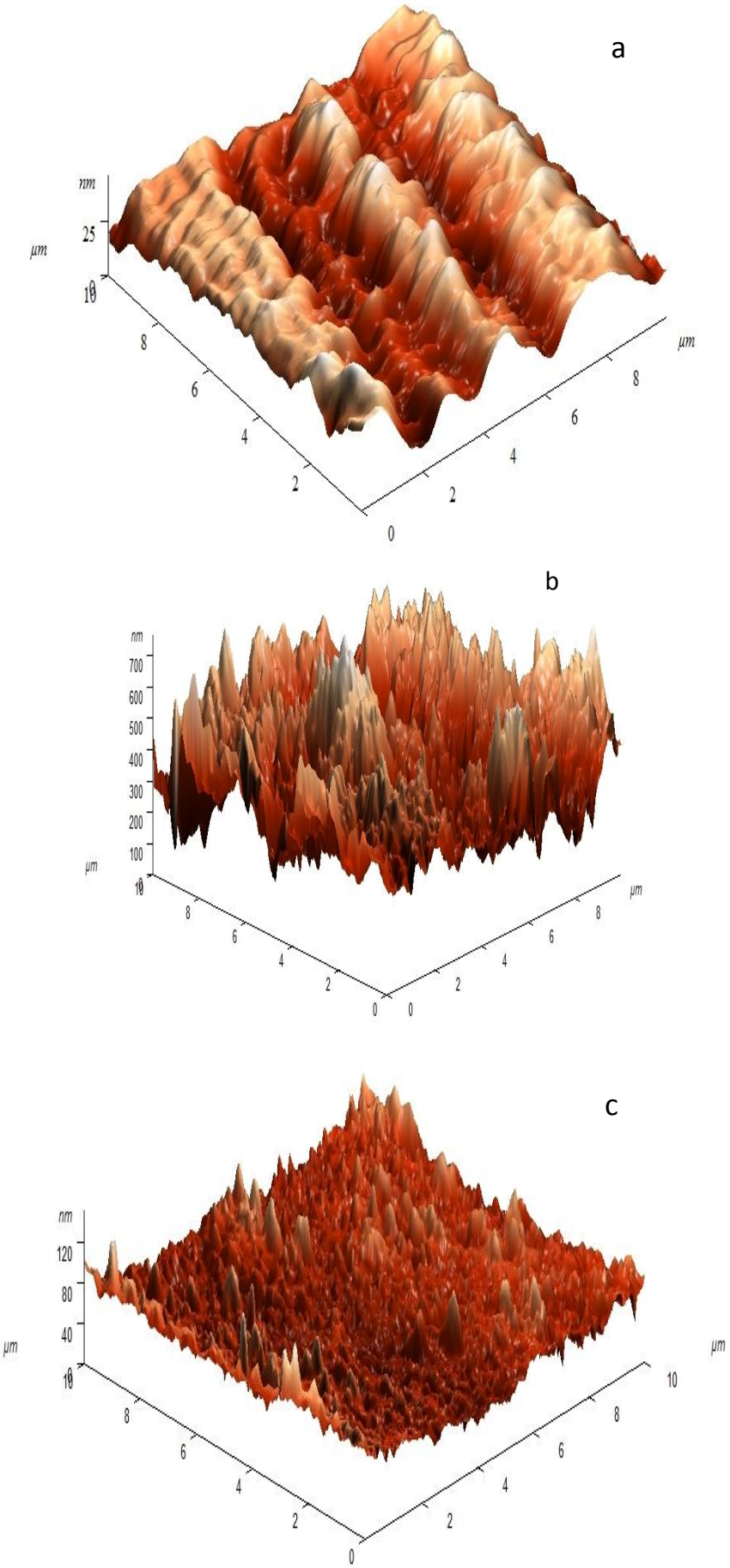
a
nm
25
0
μm
0
2
4
6
8
10
μm
b
nm
700
600
500
400
300
200
100
0
μm
0
2
4
6
8
10
μm
c
nm
120
80
40
0
μm
0
2
4
6
8
10
μm

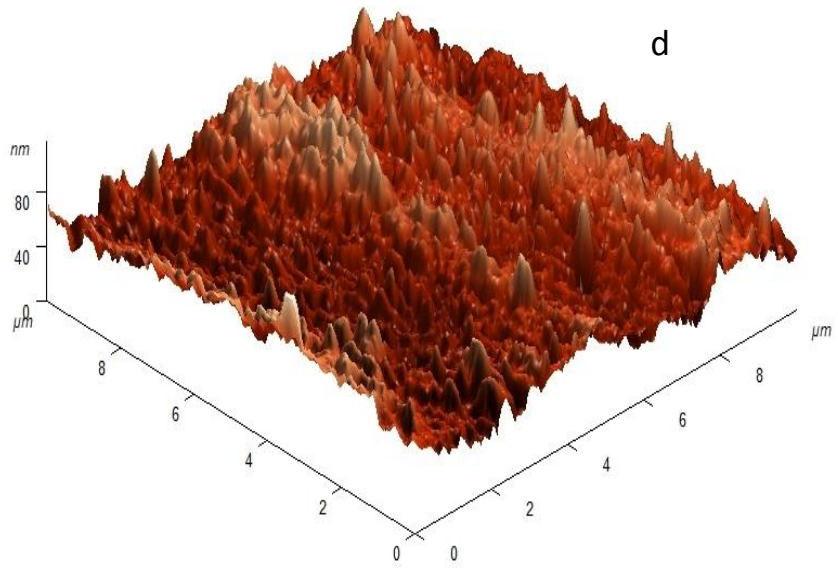

Figure 11. Atomic force micrographs of mild steel surface (a) polished mild steel, (b) mild steel in 15% HCl solution and (c) in presence of inhibitor MBTMT (d) CBTMT.

According to the frontier molecular orbital (FMO) theory of chemical reactivity, the formation of a transition state is due to interaction between HOMO and LUMO of reacting species. The smaller the orbital energy gap (ΔE) between the participating HOMO and LUMO, the stronger the interactions between two reacting species [32].

For the calculations of quantum chemical parameters such as absolute electronegativity (χ), global hardness (γ) and softness (σ) and fraction of electrons transferred from the inhibitor molecule to the metal surface (ΔN) following equations were used [33].

$$\chi = -\frac{E_{\mathrm{LUMO}} + E_{\mathrm{HOMO}}}{2} \tag{8}$$

$$\gamma = \frac{E_{\mathrm{LUMO}} - E_{\mathrm{HOMO}}}{2} \tag{9}$$

$$\sigma = \frac{1}{\gamma} \tag{10}$$

$$\Delta N = \frac{\chi_{Fe} - \chi_{inh}}{2\left(\gamma_{Fe} + \gamma_{inh}\right)} \tag{11}$$

where a theoretical value of $\chi_{\mathrm{Fe}} \approx 4.06$ eV is taken for iron and $\gamma_{\mathrm{Fe}} = 0$ is taken assuming that $I = A$ for bulk metals [33].

It was reported previously by some researchers that smaller values of ΔE and higher values of dipole moment (μ) are responsible for higher inhibition efficiency [34]. The lower values of the energy gap ΔE will render good inhibition efficiencies since the energy to remove an electron from the last occupied orbital will be minimized. According to HSAB theory hard acids prefer to co-ordinate to hard bases and soft acid to soft bases. Fe is considered as soft acid and will co-ordinate to molecule having maximum softness and small energy gap ($\Delta E = E_{\mathrm{LUMO}} - E_{\mathrm{HOMO}}$). Higher value of E_{HOMO}, μ and lower values of ΔE and E_{LUMO} for MBTMT as compared to CBTMT indicating that MBTMT has more potency to get adsorbed on the mild steel surface resulting greater inhibition tendency than MBTMT.

In present study the inhibition efficiency increases with the increasing dipole moment of the inhibitors, which could be attributed as higher polarity compounds will facilitates electrostatic interaction between the electric field due to the charged metal surface and electric moments of the inhibitors and contributes to their better adsorption by influencing the transport process through the adsorbed layer [35, 36]. Generally, ΔN shows inhibition efficiency resulting from electrons transferred from the inhibitor molecule to the iron atom. According to Lukovits et al., [37] if the value of ΔN is less than 3.6, the efficiency of inhibition increases with increasing electron-donating ability of the inhibitor at the metal surface. An improvement in electronic-releasing power was shown by replacing the hydrogen atom by electron-donating substituent ($-OCH_3$ group) in MBTMT, which improved the inhibition efficiency but at the other hand a diminishing effect has been observed by electron-withdrawing substituent (−Cl) in CBTMT. Figure 12, reveals that the HOMO location in both the inhibitors is mostly distributed in vicinity of the thiazolidine and benzylidene ring whereas LUMO location in both the inhibitors is mostly distributed in vicinity of the thiazolidine, benzylidene and benzothiazole ring, suggesting that these are the coordinating sites of the inhibitors.

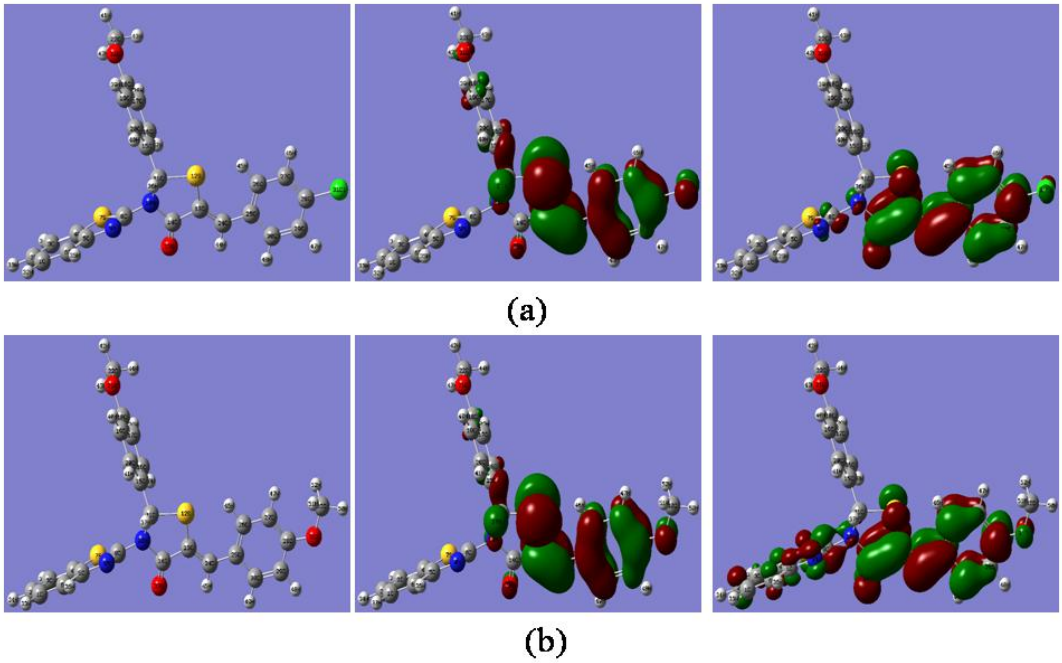

Figure 12. The optimized structure (left) and *HOMO* (center) and *LUMO* (right) distribution for molecules (a) CBTMT (b) MBTMT [H, Grey; C, Cyan; N, Blue; O, Red; Cl, green; S, Yellow].

Table 7. Quantum chemical parameters for different inhibitors

Inhibitor	$-E_{HOMO}$ (eV)	$-E_{LUMO}$ (eV)	ΔE (eV)	μ (D)	χ (eV)	γ (eV)	σ (eV^{-1})	ΔN
CBTMT	5.9834	1.0597	3.9237	4.329	3.5216	1.9619	0.5097	0.1372
MBTMT	5.5073	1.1815	2.8258	4.567	3.3444	1.4129	0.7078	0.2532

3.7. Mechanism of inhibition

Corrosion inhibition of mild steel in 15% hydrochloric acid solution by both inhibitors (MBTMT and CBTMT) can be explained on the basis of molecular adsorption. These compounds inhibit corrosion by controlling both anodic as well as cathodic reactions. In 15% hydrochloric acid solutions these inhibitors exist as protonated species. In both inhibitors the nitrogen, sulfur and oxygen atoms present in the molecules can be easily protonated in acidic solution. These protonated species adsorbed on the cathodic sites of the mild steel and decrease the evolution of hydrogen. The adsorption on anodic site occurs through π-electrons of thiazolidine, benzylidene and benzothiazole rings and lone pair of electrons of nitrogen, sulfur and oxygen atoms present in both the inhibitors which decrease the anodic dissolution of mild steel.

4. CONCLUSIONS

(1) The synthesized benzothiazole derivatives act as good corrosion inhibitor for mild steel in 15% HCl solution and inhibiting performance of MBTMT is better than CBTMT.

(2) Polarization studies showed that both tested inhibitors are predominant in cathodic nature.

(3) EIS measurements show that charge transfer resistance (R_{ct}) increases and double layer capacitance (C_{dl}) decreases in presence of inhibitors, suggested the adsorption of the inhibitor molecules on the surface of mild steel.

(4) The results obtained from SEM, EDX, AFM and Langmuir adsorption isotherm suggested that the mechanism of corrosion inhibition is occurring mainly through adsorption process.

(5) The theoretical parameters obtained by DFT calculations correlates the results of MBTMT and CBTMT obtained by experimental studies.

References

1. M. Bouayed, H. Rabaa, A. Srhiri, J.Y. Saillard, A. Ben Bachir, *Corros. Sci*. 41 (1999) 501.
2. M. Yadav, P. N. Yadav, U. Sharma, *Indian J. Chem. Technol.* 20 (2013) 363.
3. E. Stupnišek-Lisac, S. Podbršc˘ek, T. Soric, *J. Appl. Electrochem.* 24 (1994) 779.
4. F. Touhami, A. Aouniti, Y. Abed, B. Hammouti, S. Kertit, A. Ramdani, K. Elkacemi, *Corros. Sci.* 42 (2000) 929.
5. L. Tang, X. Li, L. Li, G. Mu, G. Liu, *Surf. Coat. Technol.* 201 (2006) 384.
6. M. Hosseini, S.F.L. Mertens, M. Ghorbani, M.R. Arshadi, *Mater.Chem. Phys*. 78 (2003) 800.
7. N.C. Subramanyam, B.S. Sheshardi, S.A. Mayanna, *Corros. Sci.* 34 (1993) 563.
8. S.A. Ali, M.T. Saeed, S.U. Rahman, *Corros. Sci*. 45 (2003) 253.
9. F. Bentiss, M. Lebrini, M. Lagrenee, *Corros. Sci.* 47 (2005) 2915.
10. M. Lebrini, F. Bentiss, H. Vezin, M. Lagrenée, *Corros. Sci.* 48 (2006) 1279.
11. J. Cruz, R. Martinez, J. Genesca and E. Garcia-Ochoa, *Electroanal. Chem*. 566 (2004) 111.
12. K.F. Khaled, *Electrochim. Acta* 48 (2003) 2493.
13. M. Yadav, D. Behera, S. Kumar, R. R. Sinha, *Ind. Eng. Chem. Res*. 52 (2013) 6318.
14. M. Yadav, D. Behera, U. Sharma, *Corros. Eng. Sci. Technol.* 48 (2013) 19.

15. M. Yadav, D. Behera, U. Sharma, *Arab. J. Chem.* DOI: 10.1016/j.arabjc.2012.03.011.
16. D. Shashank, T. VIshawanth, V. Balasubramaniam, V. Nagendra, P. Perumal. R. Suthakaran, *Int.J. ChemTech Res.* 1 (2009) 1224.
17. A. Dhanapala, S. R. Boopathy, V. Balasubramanian, *J. Alloys. Comp*. 523 (2012) 49.
18. M. Lebrini, F. Robert, A. Lecante, C. Roos, *Corros. Sci.* 53 (2011) 687.
19. C. Lee, W. Yang, R. G. Parr, *Phys. Rev. B*, 37 (1988) 785.
20. A. U. Ezeoke1, O. G. Adeyemi1, O. A. Akerele1, N. O. Obi-Egbedi, *Int. J. Electrochem. Sci.* 7 (2012) 534.
21. E. E. Ebenso, I. B. Obot, *Int. J. Electrochem. Sci.* 5 (2010) 2012.
22. L. F. Mar, O. O. Xometl, A. Marco, P. A. Lozada, F. J. Cruz , *Corros. Sci*. 61 (2012) 171.
23. I. Dehri, M. Ozcan, *Mater. Chem. Phys*. 98 (2006) 316.
24. X. Wang, H.; Yang, F. Wang, *Corros. Sci.* 53 (2011) 113.
25. M. Behpour, S.M. Ghoreishi, N. Soltani, M. Salavati-Niasari, M. Hamadanian, A.Gandomi, *Corros. Sci*. 50 (2008) 2172.
26. K. F. Khaled, *Electrochimca Acta* 53 (2008) 3484.
27. H.A. Sorkhabi, M.R. Majidi, K. Seyyedi, *Appl. Surf. Sci*. 225 (2004) 176.
28. M.A. Amin, K.F. Khaled, *Corros. Sci*. 52 (2010) 1762.
29. M. Lebrini, M. Lagrene´e, H. Vezin, M. Traisnel, F. Bentiss, *Corros. Sci*. 49 (2007) 2254.
30. H. Gerengi, H.I. Sahin, *Ind. Eng. Chem. Res.* 51 (2012) 780.
31. S. Ghareba, S. Omanovic, *Electrochim. Acta*. 56 (2011) 3890.
32. S. Xia, M. Qiu, L. Yu, F. Liu, H. Zhao, *Corros. Sci*. 50 (2008) 2021.
33. R.G. Pearson, *Inorg Chem* 27(1988) 734.
34. V.S. Sastri, J.R. Perumareddi, *Corrosion* 53 (1997) 617.
35. Y.M. Tang, W.Z. Yang, X.S. Yin, Y. Liu, R. Wan, J.T. Wang, *Mater. Chem. Phys.* 116 (2009) 479.
36. K. Babić-Samardžija, K.F. Khaled, N. Hackerman, *Appl. Surf. Sci.* 240 (2005) 327.
37. I. Lukovits, E.Klaman, F. Zucchi, *Corrosion* 57 (2001) 3.